Proposed method: Using the scene likeness of shots as defined above and extending the block partitioning algorithm proposed in [5] for solving linear equations, we have devised the following iterative procedure for partitioning the graph induced by the scene likeness matrix of a video into scene clusters in a way that maximises the scene likeness of shots within the same cluster and the distinction of shots between different clusters. Let C_k be the set of shots eligible to be included in cluster V_k and R be the set of shots that have not been assigned to any scene cluster.

Step 1: Set $k=1$ and $R=V$.
Step 2: Initialise V_k by moving shot s_1^k from R to V_k, where $s_1^k = \arg\max_{s_i \in R} \mathrm{L}(s_i, R)$. Set $C_k \leftarrow \{s_i | \mathrm{L}(s_i, s_1^k) = 1,\ s_i \in R\}$ and $R \leftarrow R \backslash C_k$.
Step 3: For each shot $s_i \in C_k$, if either one of the two criteria
(i) $\varphi(V_k \cup \{s_i\}) \geq \alpha$, where $\alpha \geq 0$, and
(ii) $\gamma(s_i, V_k, R \cup C_k) \geq \beta$, where $\beta \geq 1$
is satisfied, then set $n \leftarrow n+1$, move s_i from C_k to V_k (i.e., $s_n^k = s_i$), and update C_k and R as $C_k \leftarrow C_k \cup \{s_i | \mathrm{L}(s_i, s_n^k) = 1,\ s_i \in R\}$ and $R \leftarrow R \backslash \{s_i | \mathrm{L}(s_i, s_n^k) = 1,\ s_i \in R\}$. Otherwise, move s_i from C_k to R.
Repeat step 3 until C_k is empty.
Step 4: If R is not empty, set $k \leftarrow k+1$ and go to step 2.
Step 5: Set the total number of scenes $K=k$, and output scene clusters $V_1, \ldots, V_K$.

Note that in step 2 and step 3, only those shots that are similar to at least one shot in cluster V_k are included in set C_k, a constraint that speeds up the clustering procedure and makes it computationally more efficient than conventional methods. In step 3, the first criterion ensures that the connectivity of subgraph G_k remains high after the inclusion of a new shot, while the second criterion requires that, for a new shot to be included in cluster V_k, the majority of its similar shots must be in V_k. Moreover, parameters α and β can be adjusted to control the connectivity of shots within each cluster V_k. Larger the value of α, the more small and highly similar scene clusters will be formed. By increasing the value of β, a new shot can be admitted to cluster V_k only if most of its similar shots are in V_k. Based on our empirical study, setting the values of α and β in the ranges 0.6–0.9 and 1.0–2.5, respectively, can generally produce good clustering results.

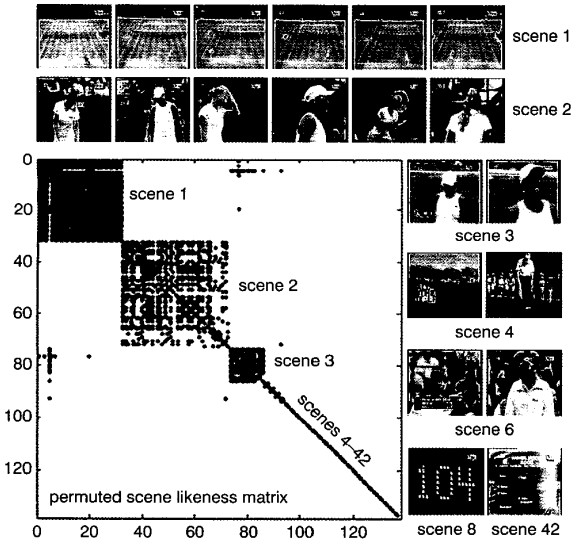

Fig. 3 *Permuted scene likeness matrix and sample shots from several clustered scenes*

Experimental results: We have applied the proposed method to a variety of videos and obtained promising results. Fig. 3 shows the scene likeness matrix of the 137-shot Tennis test video and the sample shots from several clustered scenes; the rows and columns of the matrix have been permuted according to the scene clustering results obtained by the proposed method, and each dot (i, j) in the matrix indicates that the two corresponding shots cover a similar scene. It can be seen that shots of similar scenes are grouped as dense blocks along the diagonal of the permuted scene likeness matrix. In particular, the first three clusters cover the scenes that appear repeatedly over the test video: wide-angle views of the court (scene 1), close-up views of the players (scene 2), and medium/close-up views of the players and the court (scene 3). The remaining clusters mainly consist of only one or two shots of transition scenes or commercials breaks (scene 4 to scene 42).

Conclusion: In this Letter, we formulate the clustering of video scenes as a problem of graph partitioning. While conventional methods such as k-means clustering and hierarchical clustering have been widely used to group shots into different scenes, graph-theoretic techniques have not been well exploited for this task. We show that an efficient graph-theoretic method can be designed to cluster video shots into scenes, particularly when the number of scene clusters is not known *a priori*.

24 March 2003
Electronics Letters Online No: 20030536
DOI: 10.1049/el:20030536

Yap-Peng Tan and Hong Lu (*School of Electrical and Electronic Engineering, Nanyang Technological University, Singapore, Block S1, Nanyang Avenue, Singapore 639798, Singapore*)

E-mail: eyptan@ntu.edu.sg

References

1 HANJALIC, A., and ZHANG, H.: 'An integrated scheme for automated video abstraction based on unsupervised cluster-validity analysis', *IEEE Trans. Circuits Syst. Video Technol.*, 1999, **9**, (8), pp. 1280–1289
2 YEUNG, M., YEO, B.-L., and LIU, B.: 'Extracting story units from long programs for video browsing and navigation'. IEEE Intl. Conf. on Multimedia Computing and Systems, Hiroshima, Japan, 1996 pp. 296–305
3 WANG, X., and KUO, C.-C.: 'Color distribution analysis and quantization for image retrieval', *Proc. SPIE*, 1996, **2670**, pp. 8–16
4 DUDA, R.O., HART, P.E., and STORK, D.G.: 'Pattern classification' (Wiley-Interscience, 2000, 2nd edn.)
5 O'NEIL, J., and SZYLD, D.B.: 'A block ordering method for sparse matrices', *SIAM J. Sci. Stat. Comput.*, 1990, **11**, (5), pp. 811–823

Experimental demonstration of evanescent coupling from optical fibre tapers to photonic crystal waveguides

P.E. Barclay, K. Srinivasan, M. Borselli and O. Painter

Experimental results demonstrating nearly complete mode-selective evanescent coupling to a photonic crystal waveguide from an optical fibre taper are presented. Codirectional coupling with 98% maximum power transfer to a photonic crystal waveguide of length 65 μm and with a coupling bandwidth of 20 nm is realised.

Introduction: The control of the confinement and dispersion of light offered by photonic crystals (PCs) allows the realisation of novel optical devices such as high-Q microcavities, nanoscale lasers, waveguides, and add-drop filters. Because of their small length-scale and complex mode-shape in comparison to either standard optical fibre modes or free-space diffraction-limited optical beams, the efficient coupling of light into PC devices has proven challenging. Evanescent coupling to a photonic crystal waveguide (PCWG) from an optical fibre taper overcomes this obstacle by matching momentum rather than spatial overlap, allowing highly efficient power transfer between a single mode of each waveguide [1]. When the fibre taper is positioned parallel and close to a PC waveguide, its small diameter ($\sim\lambda$) permits the evanescent tail of its field to interact with the PC waveguide. If there exists a pair of modes (one in each waveguide) which are phase matched and which have appropriate *transverse* spatial overlap, nearly complete power tranfer over distances as short as several tens of PC lattice constants is theoretically possible. Here we present experimental data demonstrating this result.

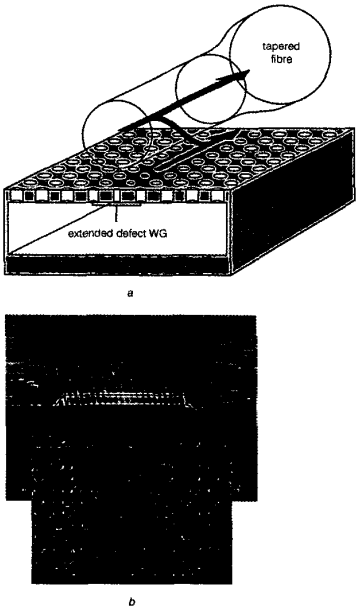

Fig. 1 *Schematic diagram and SEM images*
a Schematic diagram of coupling scheme
b SEM images of typical PC defect waveguide

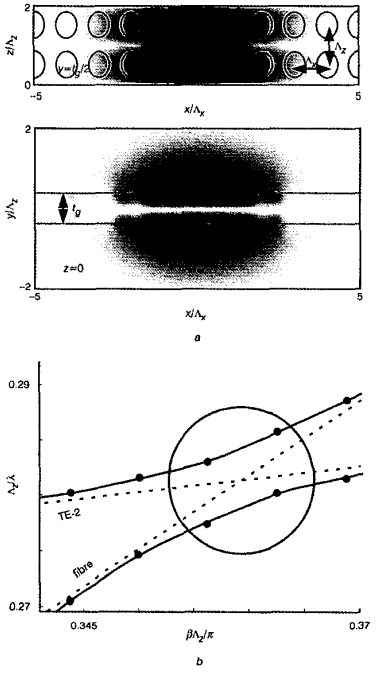

Fig. 2 *TE-2 valence band guided mode magnetic field profile ($|B_y|$), and PCWG-fibre bandstructure near phase matching point*
a TE-2 valence band guided mode magnetic field profile ($|B_y|$)
b PCWG-fibre supermode bandstructure near phase matching point
Approximate dispersion of uncoupled waveguide modes indicated by dashed lines
Taper-PCWG gap is Λ_x in this calculation

Design, fabrication and test setup: Fig. 1*a* shows a schematic of the coupling scheme, and Fig. 1*b* shows SEM images of the PC waveguide considered here. The PCWG was fabricated from a silicon-on-insulator (SOI) wafer by dry etching a compressed square lattice ($\Lambda_z = 430$ nm, $\Lambda_x/\Lambda_z = 0.8$) of air-holes through a 340 nm thick silicon layer residing on top of a 2 μm silicon-dioxide layer, and then selectively wet etching the underlying silicon dioxide using a hydroflouric acid solution. The resulting undercut structure is essential to prevent the fibre taper from radiating into the substrate when it is placed close to the PCWG. The defect waveguide was formed by introducing a lateral grading in the hole radius similar to the PC defect cavities studied in [2]. Fig. 2*a* shows the finite-difference time-domain (FDTD) calculated field profile of the valence band PCWG defect mode that couples strongly to the fibre taper mode. The PCWG mode is a second-order (in the vertical direction) TE-like mode, and is labelled TE-2. Fig. 2*b* shows the supermode calculation of the taper-PCWG bandstructure, where the coupling region of the fundamental taper mode and the TE-2 mode has been circled. The length of PCWG studied here was 150 lattice periods long, limiting the length of the coupler to 65 μm.

An approximately 1.2 μm diameter fibre taper was fabricated by simulateneously heating and stretching a segment of standard singlemode telecommunication fibre. The fibre section containing the fibre taper was then spliced into a fibre link containing a laser source, polarisation rotating paddle wheels, a 2×2 splitter, and a photodetector. The laser source used in this experiment was a scanning external cavity laser with a wavelength range of 1565–1625 nm and a resolution of 1 pm. The fibre taper was positioned above and parallel to the PCWG using a stage with 50 nm resolution along the vertical axis. A fibre-optic broadband (40 nm) 99 : 1 2×2 splitter was used on the input side (before the taper-PCWG coupling region) of the fibre taper to monitor the *back-reflected* signal. On the output side (after the taper-PCWG coupling region) the fibre taper was connected directly to a photodetector which measured the *forward transmitted* signal.

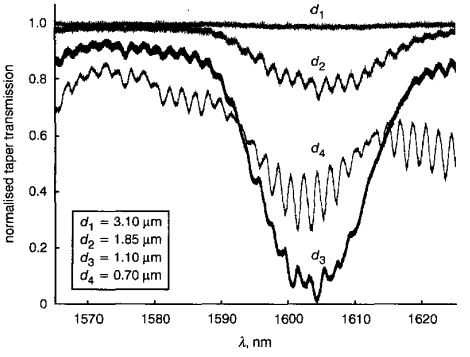

Fig. 3 *Taper transmission against wavelength for varying taper-PCWG vertical gap*

Results: Fig. 3 shows a wavelength scan of the transmitted signal for the fibre taper positioned at a series of heights above the centre of the PCWG. For a taper-PCWG gap of 3.10 μm (d_1) the taper mode does not couple to the PCWG and has unity transmission over all wavelengths in the scan. As the taper-PCWG gap is closed and reaches 1.85 μm (d_2), one begins to see resonant coupling to the PCWG about the phase matched point. At a gap of 1.10 μm (d_3) we obtain maximum power transfer between the taper mode and the PCWG with a taper transmission minimum below 2%. With the gap further decreased to 0.70 μm (d_4) the transmission begins to recover and two side-lobes in the transmission become prominent. The transmission does not decrease monotonically with gap distance, but rather oscillates with two local minima occuring before the fibre taper finally touches the PC. This Rabi-flopping power transfer indicates that the coupling is co-directional. Superimposed upon the codirectional coupling curve there are Fabry-Perot (FP) resonances resulting from reflections at the ends of the PCWG (the 65 μm long PCWG is terminated abruptly into a non-patterned silicon membrane region). By examining this high frequency (~2 nm period) structure of the transmission data, the group index of the PC mode and the reflectivity of the PC waveguide termination are estimated to be 9.5 (compared to the theoretical value of 8.5 from Fig. 2) and 12%, respectively. A simple two-port model is then used to fit the transmission data as a function of transverse coupling strength, $\kappa_\perp$, and effective coupler length, L_c (the group index of the fibre taper mode was taken to be 1.45, roughly equal to the refractive index of the silica). The normalised effective coupling strength, $\kappa_\perp L_c$, was determined from the depth of the minimum in

the transmission curve, and the effective coupling length was fit so as to match the bandwidth of the main lobe in the coupling curve. By fitting the coupling curves over a wide range of taper-PCWG gaps (over a full Rabi-flop) we found that L_c was approximately 20 μm in length, significantly shorter than the actual PCWG length. We believe this to be a result of variation along the length of the PCWG in the phase-velocity of the PCWG mode due to fabrication errors and/or variation in the transverse coupling strength ($\kappa_\perp$) as a result of bowing or angle misalignment of the fibre taper. This is further coroborated by the supression of the side-lobes in our coupling curve [3].

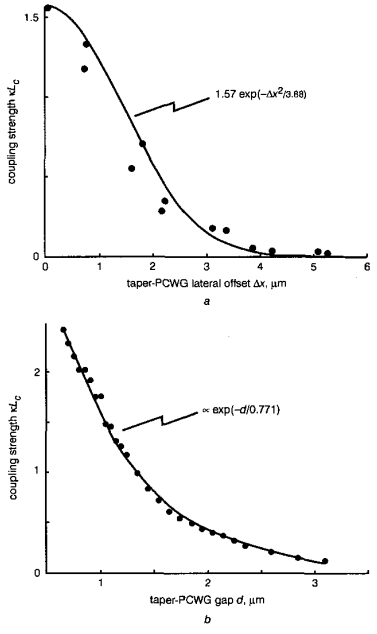

Fig. 4 *Normalised coupling strength against taper-PCWG lateral displacement and against taper-PCWG vertical gap*

a Against taper-PCWG lateral displacement *b* Against taper-PCWG vertical gap

At maximum coupling the full-width half-maximum (FWHM) bandwidth of the main lobe of the transmission curve is roughly 20 nm, centred about $\lambda = 1604$ nm. Note that the off-resonance transmission recovers nearly fully for this coupling gap, indicating there is very little scattering loss occuring at the taper-PCWG interface and consequently efficient power transfer to the PCWG (>98%) at the phase-matched point. The back-reflected signal (generated by circulating power in the PCWG) is also found to be a maximum in this case with a similar wavelength dependence as for the taper transmission. Keeping the vertical taper-PCWG separation fixed at 1.10 μm, Fig. 4*a* shows the normalised effective coupling strength against lateral position of the fibre taper relative to the centre of the PCWG. From this plot one sees that the coupling is strongest within 1 μm of the PCWG defect region with an approximately Gaussian dependence upon lateral offset, confirming that the taper mode is coupling to a confined PCWG defect mode. The normalised effective coupling strength against vertical taper-PCWG gap is plotted in Fig. 4*b*. The coupling strength was also found to be very polarisation sensitive, and could be extinguished by over 90% by varying the polarisation of the source. This is due to the strong in-plane polarisation of the PCWG mode.

These results are the first demonstration of highly efficient coupling to a confined PCWG mode from a fibre taper, and represent a first step towards using evanescent coupling to efficiently interface with planar PC devices.

26 March 2003
Electronics Letters Online No: 20030565
DOI: 10.1049/el:20030565

P.E. Barclay, K. Srinivasan, M. Borselli and O. Painter (*Department of Applied Physics, California Institute of Technology, Pasadena, California 91125, USA*)

References

1 BARCLAY, P.E., SRINIVASAN, K., and PAINTER, O.: 'Evanescent coupling between photonic crystal slab waveguides and silica optical fibers'. in *PECS-IV: International Workshop on Photonic and Electromagnetic Crystal Structures*, University of California, Los Angeles, 2002, IPAM, p. 38

2 SRINIVASAN, K., and PAINTER, O.: 'Momentum space design of high-Q photonic crystal nanocavities in two-dimensional slab waveguides', *Opt. Expr.*, 2002, **10**, (15), pp. 670–684

3 ALFERNESS, R.C., and CROSS, PETER S.: 'Filter characteristics of codirectionally coupled waveguides with weighted coupling', *IEEE J. Quantum Electron*, 1978, **14**, (11), pp. 843–847

Lasing at bend, branch and intersection of photonic crystal waveguides

K. Inoshita and T. Baba

The authors report room temperature lasing by pulsed photopumping at line and point composite defects, i.e. a 60°-bend, a Y-branch and an intersection of single line defect waveguides, in a GaInAsP photonic crystal slab. The lasing wavelength was different from the simple line defect lasing mode. This indicates that such waveguide components act as microcavities with localised modes.

Room temperature lasing by pulsed photopumping has been reported for point defects [1–4] and a line defect [5] in a GaInAsP photonic crystal (PC) slab. In this study, we investigated point and line composite defects. Composite defects here mean a bend, a branch and an intersection of single line defect PC waveguides, as shown in Fig. 1 and are different from those in [6]. These waveguide components break the symmetry of the line defect. Therefore, they act as microcavities, although they are open towards free space through the line defects. Previously, we performed a finite difference time domain (FDTD) simulation and found that such composite defects maintain well-localised modes and allow a good mode selectivity [7]. We also fabricated some composite defects in a GaInAsP PC slab, and confirmed their mode selectivity by comparing the photoluminescence spectra with those of simple point defects [7]. In this Letter, we report the lasing in these composite defects.

In the fabrication, we used an epitaxial wafer with a GaInAsP compressively strained quantum well active layer of 243 nm in total thickness. The fabrication process was (i) Ti and Ni evaporations on the wafer as an etching mask, (ii) electron beam lithography and pattern transfer to the metals, (iii) the hole opening by Cl_2/Xe inductively coupled plasma etching and (iv) the PC slab formation by HCl selective etching. Fig. 1 shows top views of the composite defects fabricated in this way. The whole PC has a hexagonal shape and was 20–25 μm in width. Line defects were connected to the end of the PC. The lattice of the PCs was triangular, and the lattice constant a was 0.40–0.48 μm. The hole diameter $2r$ was 0.20–0.30 μm. They are typical values that provide a photonic bandgap for the transverse-electric-like polarisation.

In the measurement, the sample was placed on a metal submount without bonding. Laser diode light of 980 nm wavelength from a singlemode fibre was focused and irradiated to the sample at room temperature. The diameter of the focused spot was ~5 μm at $1/e^2$ of the peak intensity. The laser diode was driven by pulsed current. The typical duty ratio of the pulse was 0.015%, but similar results were obtained for 0.98%. The light output from the PC laser was collected to another detection multimode fibre, and analysed by an optical spectrum analyser. Output against irradiated power characteristics and the corresponding spectra of PC lasers are shown in Figs. 2 and 3, respectively. In composite defects, the output power exhibited a sudden rise with a spectral narrowing at an irradiated power of 2.5 mW, and the peak intensity of the spectrum became over 20 dB higher than the background level. Thus the lasing was confirmed. Since the focused spot was fully smaller than the whole PC, the lasing was thought to be due to localised modes. When the focused spot was moved from the 60°-bend to the PC slab without defects, such a lasing was not observed. When the spot was moved to the simple line defect, the lasing was observed, as shown by closed squares in Fig. 2, at ~20 nm shorter wavelength than that for the 60°-bend. The lasing at the line defect is explained by the band-edge mode, [5] while the lasing at the 60°-bend is explained